Geomechanics and Engineering, *Vol. 23, No. 4 (2020) 351-364*
DOI: https://doi.org/10.12989/gae.2020.23.4.351

3D numerical investigation of segmental tunnels performance crossing a dip-slip fault

Milad Zaheri[1a], Masoud Ranjbarnia[*1] and Daniel Dias[2,3,4b]

[1]*Department of geotechnical Engineering, Faculty of civil engineering, University of Tabriz, 29 Bahman Blvd, Tabriz, Iran*
[2]*School of Automotive and Transportation Engineering, Hefei University of Technology, Hefei, China*
[3]*Grenoble Alpes University, Laboratory 3SR, 38401 Grenoble Cedex 9, France*
[4]*Antea Group, Anthony, France*

(Received July 11, 2019, Revised October 25, 2020, Accepted November 4, 2020)

Abstract. This paper numerically investigates the effects of a dip-slip fault (a normal or a reverse fault) movement on a segmental tunnel which transversely crosses either of this kind of faults. After calibration of the numerical model with results from literature of centrifuge physical tests, a parametric study is conducted to evaluate the effects of various parameters such as the granular soil properties, the fault dip angle, the segments thickness, and their connections stiffnesses on the tunnel performance. The results are presented and discussed in terms of the ground surface and tunnel displacements along the longitudinal axis for each case of faulting. The gradient of displacements and deformations of the tunnel cross section are also analyzed. It is shown that when the fault dip angle becomes greater, the tunnel and ground surface displacements are smaller, in the case of reverse faulting. For this type of fault offset, increasing the tunnel buried depth causes tunnel displacements as well as ground surface settlements to enhance which should be considered in the design.

Keywords: segmental tunnel; normal fault; reverse fault; numerical simulation; soil

1. Introduction

Some cities around the world are located in seismic belts and encompassed by various active faults. Thus, it is necessary to study some aspects of fault movements on the stability of under construction or built structures. The potential damage of structures is then associated with several factors such as the fault type, the fault movement rate (depending on the released energy from the Earth's lithosphere), and the distance to the fault location.

Tunnels are built to simplify the transportation of people or goods, and therefore, their construction might be inevitable in the vicinity of active faults. This unfavorable condition can induce stability problems (e.g., tunnel damages due to the Kobe, San Francisco, and Chi-Chi earthquakes (Lin *et al.* 2007)).

Most studies have been focused on the investigation of fault movements effects on free field (Lin *et al.* 2007, Loukidis *et al.* 2009) and on shallow or deep foundations (Anastasopoulos and Gazetas, 2007, Anastasopoulos *et al.* 2008, Bransby *et al.* 2008a, b, Ng *et al.* 2014, Soomro *et al.* 2017). Few efforts have been devoted to study the issue of urban shallow tunnels and active faults. Table 1 summarizes the studies by numerical and physical models to investigate the recent issue.

Table 1 The previous studies on the effects of the faulting on tunnels

Study	Method of study	Fault type	Lining type	Fault plane-Tunnel axis
Gregor *et al.* (2007)	3D Numerical	Oblique	Segmental	Transverse
Lin *et al.* (2007)	Physical (by a centrifuge) and numerical	Reverse	Shotcrete	parallel
Wang *et al.* (2012)	3D Numerical	Reverse, Normal, and strike-slip	Shotcrete	Transverse
Baziar *et al.* (2014)	Physical (by a centrifuge)	Reverse	Shotcrete	parallel
Baziar *et al.* (2016)	2D Numerical	Reverse	Shotcrete	parallel
Kiani *et al.* (2016)	Physical (by a centrifuge)	Normal	Segmental	Transverse
Cai *et al.* (2019)	Physical (by a centrifuge) and numerical	Normal	Shotcrete	Transverse

Lin *et al.* (2007) studied the influence of a fault movement on a shotcreted tunnel where the fault plane was parallel to the tunnel longitudinal axis. The parametric study was carried out by using small scale centrifuge tests and by 2D numerical models. The effect of various parameters such as the fault angle as well as the tunnel location respect to the fault tip was evaluated. It was observed that further the distance of the fault plane to the tunnel location is and lower are the induced damages. Gregor *et al.* (2007) studied, using a three-dimensional

*Corresponding author, Associate Professor
E-mail: M.ranjbarnia@tabrizu.ac.ir
[a]Ph.D. Student
E-mail: Miladzaheri@tabrizu.ac.ir
[b]Professor
E-mail: daniel.dias@ujf-grenoble.fr

ISSN: 2005-307X (Print), 2092-6219 (Online)

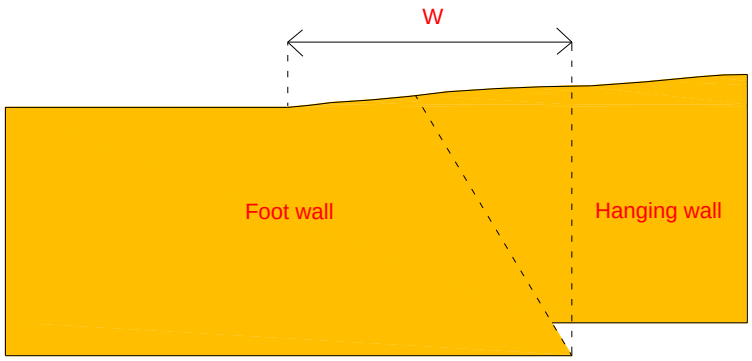

Fig. 1 Hanging wall, foot wall, and parameter W

numerical modelling, the stability of twin tunnels crossing an oblique fault (including a normal and strike-slip fault). They showed that the soil mass and water can flow into the segmental tunnels after faulting, which causes several problems (e.g., stability problems). In the other attempt, Wang *et al.* (2012) numerically investigated the interaction between a deep tunnel with continuous lining (i.e., shotcrete) and different types of faulting. The strike-slip fault movement imposes a higher level of damage to the tunnel than the other kind of faults. Baziar *et al.* (2014, 2016) studied, by a centrifuge physical model, the case of a reverse fault offset which crosses a shotcreted tunnel. They also simulated this problem using a numerical method. As the numerical model was a two dimensional one, it was only possible to perform a parametric study on the cases where the fault plane was parallel to the tunnel longitudinal axis. The results indicated that the soil elastic modulus is the most critical parameter controlling the stability of tunnels. As well, increasing the soil stiffness causes the faulted zone on the ground surface to reduce. Kiani *et al.* (2016) studied the effects of a normal transverse fault on a segmental tunnel embedded in a dry sandy soil by small scale centrifuge tests. Two different fault dip angles and tunnel depths were modeled. Their effects on the tunnel deformations were studied. It was found that increasing the tunnel overburden leads to a decrease of the impacted number of tunnel rings. However, the effects of the soil mechanical properties and the segments connections were not investigated due to some limitations associated to the physical model. Recently, Cai *et al.* (2019) investigated the deformation of a tunnel due to the normal faulting by means of small-scale centrifuge model tests as well as by numerical simulations. The supporting system was made of a shotcrete layer although it was stated as to be segmental type. In fact, the stiffness reduction method was used to simulate the segments behavior. Thus, the details of the segments connections and their separation were not considered. These parameters can have a significant effect on the stability of tunnels, and on its interaction with the soil mass.

The problem of fault movements' effects on segmental tunnel has still some gaps. In addition to the above-mentioned defects associated to the impact of the segments connections, the performance of a segmental tunnel transversely crosses by a fault plane was not still properly discussed. Furthermore, the effects of the fault dip angle, segments thickness, tunnel depth, and geo-mechanical properties of the soil mass on the tunnel performance for each case of normal or reverse faulting are not sufficiently clearly presented to be easily compared.

In this paper, a three dimensional (3D) numerical model is developed and validated by the results of centrifuge physical tests (Kiani *et al.* 2016 and Kiani 2016). Afterwards, a parametric study is performed to investigate the effects of several parameters.

2. Numerical modeling procedure

2.1 Definitions and general assumptions

Two kind of faults are considered in the following numerical work. If the hanging wall moves upward relative to the foot wall, the fault is called Reverse, meanwhile, the hanging wall moves downward relative to the foot wall, the fault is Normal (see Fig. 1). The horizontal distance between the intersection of the fault plane and the bedrock. The location of the surface outcropping (location where the ground displacement induced by the fault offset is equal to zero) is called W (see Fig. 1).

Simulation of these fault offsets is carried out using a finite difference code FLAC^{3D}. The following procedure is adopted:

1st step: The numerical model is set up, and the boundary conditions, as well as the initial stresses (taking into account of the gravity) are assigned. A parametric study on the mesh size and boundary locations is conducted to minimize the mesh and boundary effects on the results. Displacements are fixed normally to the vertical boundaries and vertical faces of each side, and displacements at the bottom of the model are fixed in the vertical direction (Fig. 2). Initial horizontal and vertical stresses are assigned to the model to simulate the gravity action,

2nd step: The tunnel is excavated, and the segments are installed. Then, the system is brought to equilibrium. Finally, the displacements and velocities are set to zero,

3rd step: The velocities are specified to the boundaries of the hanging wall (the moving part of the model) to move it in the fault direction. All of the tests are performed in large strain conditions (the nodal coordinates are updated at each calculation step).

To simulate the shearing mechanism between the fault

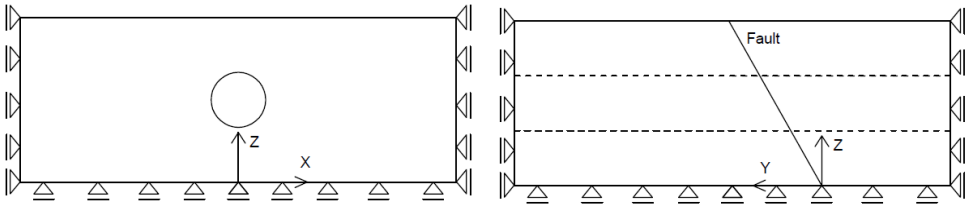

Fig. 2 Boundary conditions

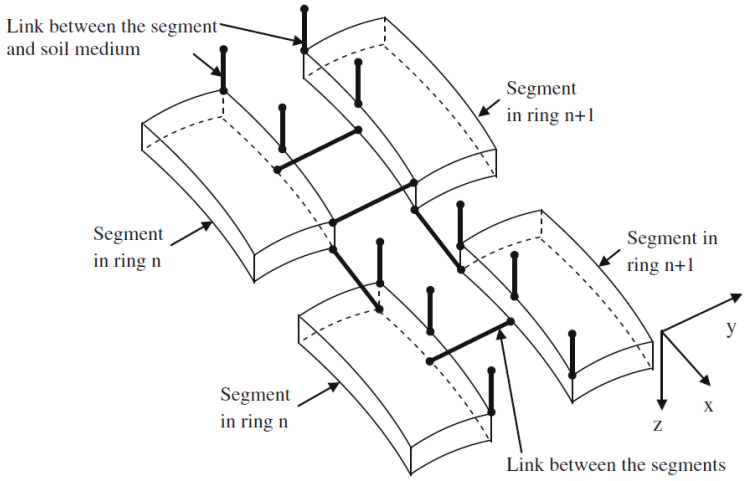

Fig. 3 Ring joint scheme (Do *et al.* 2014d)

sides, an interface element is introduced to consider the shearing and sliding mechanism. The shearing behavior is governed by a linear elastic perfectly plastic constitutive model (considering the Mohr-coulomb shear failure criterion (Itasca 2005)) in which its properties such as the cohesion, the friction angle, and the dilation angle are assumed to be the same as the soil mass ones. The normal stiffness and the shear stiffness values are taken as ten times the equivalent stiffness value proposed by Eq. (1) (Itasca 2005).

$$\max\left[\frac{K+\frac{4}{3}G}{\Delta z_{min}}\right] \quad (1)$$

As seen, these stiffnesses are a function of the shear modulus (G), the bulk modulus (K), and the smallest dimension of the adjacent zone in the normal direction of the fault (Δz_{min}) (Itasca, 2005, Do *et al.* 2014, Ranjbarnia *et al.* 2020, Zaheri *et al.* 2019, 2020). As there may be different materials in the adjacent of an interface, the max [.] notation represents the maximum value over all zones adjacent to it.

In the second step, the tunnel with a diameter of 5.9 meters is excavated, and precast concrete segments are installed as the supporting system. Six segments are installed at each ring where the joints in the odd rings are located at angles of 0°, 60°, 120°, 180°, 240°, and 300° and those of even rings are located at angles of 30°, 90°, 150°, 210°, 270°, and 330° (measured clockwise from the tunnel crown). The width of the lining ring is considered equal to 1.5 m.

These segments are simulated by liner elements which have a linear-elastic behavior. In fact, these segments can exhibit an elasto-plastic behavior, however, it is only possible to assign a linear elastic behavior in FLAC^{3D} (Itasca 2005, Do *et al.* 2013, 2014a, b, c, d, e, 2015). Each node of a liner structural element has two links; one permits to connect the segments together, and the other links the segment to the soil mass (Fig. 3).

To simulate the interaction between segments, as described by Do *et al.* (2013, 2014a, b, c, d and e, 2015, 2018), double node connections which include six degrees of freedom are considered at the joints in tangential and axial directions. For each of these degrees, one spring must be assigned i.e., three translational and three rotational components in the x, y, and z directions. The following four attachment conditions can be assigned to each of these springs: a) rigid; b) free; c) linear spring characterized by a stiffness factor; and d) bi-linear spring characterized by a stiffness factor and by a yield strength. In this study, the connections in the tangential direction are represented by a set composed of an axial stiffness (K_A), a radial spring (K_R), and a rotational spring (K_θ) (Do *et al.* 2013, 2014a, b, c, d, e and f, 2015) as shown in Fig. 4(a). A bi-linear relation is assumed to these stiffnesses where their values are computed by the method of Do *et al.* (2013). However, in the tangential direction (between segments in a ring), the attachment conditions are assumed to be rigid for the translation component in the y direction, and two rotational components around the x and z directions (in the local coordinate system). As seen in Fig. 4(b), the connection in the axial direction (between adjacent rings) is represented by a set composed of an axial stiffness (K_{AR}), a radial spring (K_{RR}), and a rotational spring ($K_{\theta R}$) (Do *et al.* 2014d, e, 2015). A similar assumption is also made in the axial

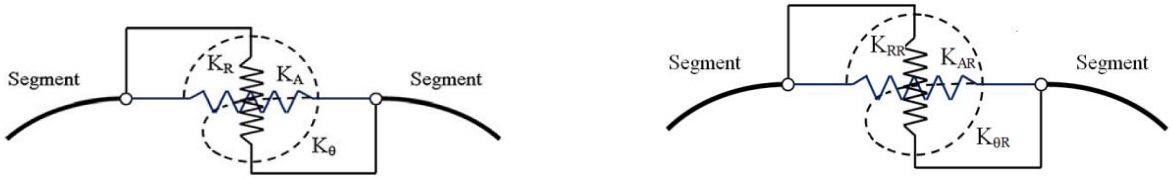

(a) (b)

Fig. 4 Stiffnesses in the axial, radial, and rotational directions (a) between segments of a ring and (b) between adjacent rings (Do *et al.* 2014d)

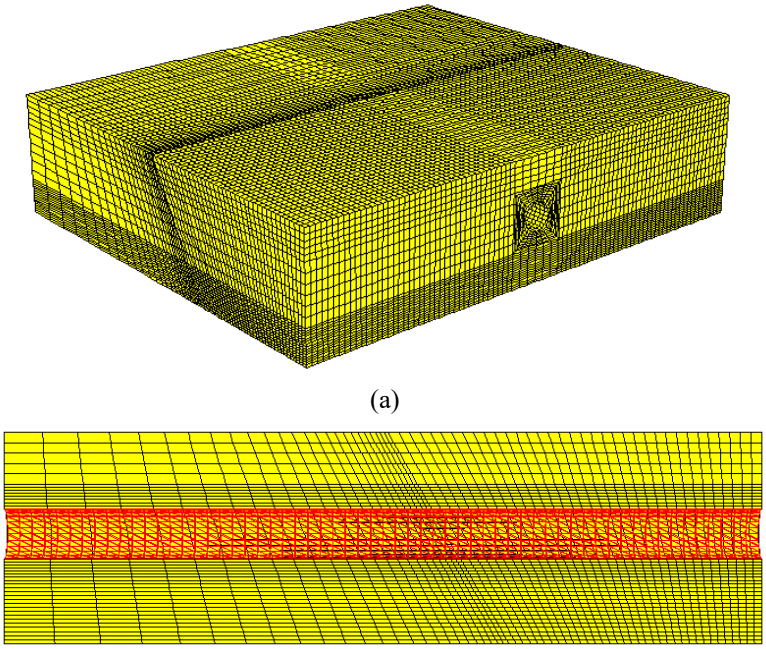

(a)

(b)

Fig. 5 Perspective view of the model and mesh (a) 3D view and (b) model along the tunnel axis

direction (between rings). These assumptions have no effect on the results according to the geometric state of the fault plane respect to the segmental tunnel axis.

To model the interaction between a segment and the medium, 100 times of the equivalent stiffness of Eq. (1) is chosen as the liner-zone interface stiffness (the normal stiffness (K_n) and the shear stiffness (K_s)). This is because Eq. (1) strictly applies only to a planar surface and if the surface is curved, this equation should be increased by a factor of 10 to 100 (Itasca 2005).

After installation of the segments, the system is brought to equilibrium, and then the displacements and velocities are set to zero.

The final step of the numerical model is the simulation of the fault offset. Quasi-static conditions are considered for all of the analyses which implies that the seismic wave propagation on the tunnel is not considered. To model the fault offset, velocities are assigned to the hanging wall boundaries in a given number of calculation steps as depicted in Fig. 1. If V and d respectively are the velocity and the applied fault displacement, then the number of steps (N) will be equal to $N = \frac{d}{V}$ (Itasca 2005, Ranjbarnia *et al.* 2020, Zaheri *et al.* 2020).

All of the required displacements were recorded by using FISH programming language.

2.2 Verification of the numerical model

After performing the parametric study in the first step of numerical simulation, the model dimensions were set to 112 m wide (X direction), 90 m long (Y direction, tunnel axis direction), and 25 m high (Z direction) while consisting around 160000 zones (Fig. 5). To validate the finite difference model, the numerical results are compared with those obtained from the centrifuge tests conducted by Kiani *et al.* (2016) and by Kiani (2016).

The experimental tests were performed on a segmental tunnel embedded in sand after dip-slip faulting. The tests conducted in these studies have been carried out under a 50 g centrifugal acceleration and the faults offset was selected as 2.5 meters (in prototype). The soil friction angle of this sand (Firoozkuh sand) was 37° and the density, elastic modulus, cohesion, and Poisson's ratio of this soil were respectively 1630 kg/m^3, 20 MPa, 0 kPa, and 0.3 (Kiani *et al.* 2016, Kiani 2016).

In the numerical simulation, the linear elastic perfectly plastic constitutive model with a shear failure criterion of

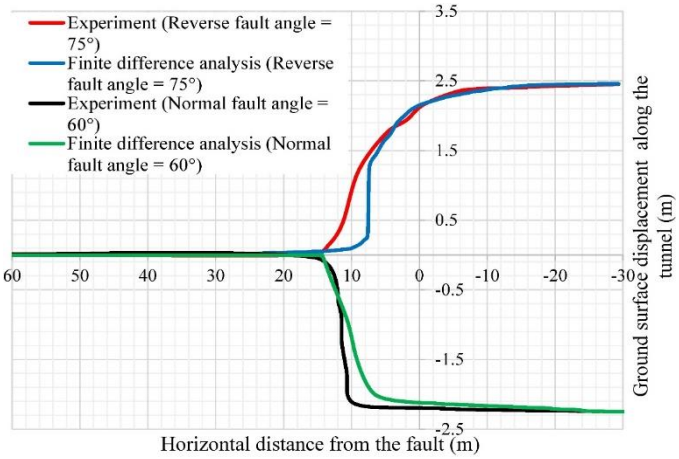

Fig. 6 Ground surface displacements in the numerical method and the experimental method

the Mohr-Coulomb type was assigned to the medium to simulate the behavior of this soil. As well, the segmental tunnel (with the tunnel external diameter (D) of 5.9 m) properties were as follows: density = 2600 kg/m^3, elastic modulus = 20 GPa, and Poisson's ratio = 0.28 (Kiani *et al.* 2016, Kiani 2016), which all were assigned to the numerical model. The friction angle between segments and medium was considered as 2/3 of the soil friction angle. Finally, the velocities were applied in N steps to the boundaries of the hanging wall in the direction of the fault. The number of steps for the reverse and for the normal faulting was chosen respectively equal to 1700 and 15000.

The ground displacements in the numerical simulation after both the normal and reverse faulting were compared with that obtained in the experimental method. As an example, Fig. 6 shows the results of a case reverse faulting (with the angle 75° and the overburden height 0.75D) and normal faulting (with the angle 60° and the overburden height 1D) for the experimental and numerical models. The results of the two simulations are very similar and in good agreement. Furthermore, the comparison is made for the maximum tunnel displacements i.e., 0.25 meters is obtained for the numerical simulation against 0.256 meters by physical model for the case of reverse faulting. The same value of 2.5 meters is obtained for the numerical and the physical model for the case of normal faulting.

Thus, the numerical model can be considered as validated and in the next section a parametric study can be conducted.

3. Parameters and input data for the parametric study

Table 2 shows the 18 investigated cases for each fault type obtained by multiplying the three tunnel depths, by the two soil types (defined as dense and loose soils), and by the three values of the friction angle. For each of soil types, a single value of the soil density and the soil elastic modulus (E_s), and three values of the friction angle were adopted. It should be noted that the values of these parameters are different from the centrifuge physical tests. In other words, new cases were considered in the parametric study.

Table 2 Properties of the cases used in the parametric study

Parameter	Symbol	Unit	Value
Fault type	-	-	Normal - Reverse
Soil type	-	-	Loose soil, Dense soil
Soil elastic modulus	E_s	MPa	15, 40
Soil peak friction angle	$\emptyset_{peak}$	◦	(24, 28, 30), (35, 36, 38)
Soil density	ρ_s	kg/m^3	1500, 1800
Tunnel depth	H	m	10, 12, 14

In the analyses, the following assumptions were made for each type of soil:

• The strain-hardening/softening constitutive model was considered for the dense soil in which the friction angle ($\emptyset$) and the dilation angle (Ψ) were a bilinear function of the shear plastic strain (γ^P).

$$\emptyset = \begin{cases} \emptyset_{peak} - \dfrac{(\emptyset_{peak} - \emptyset_{res})\gamma^P}{\gamma_f^P}, & \text{For } 0 \le \gamma^P < \gamma_f^P \\ \emptyset_{res}, & \text{For } \gamma^P \ge \gamma_f^P \end{cases} \quad (2)$$

$$\Psi = \begin{cases} \Psi_{peak}(1 - \dfrac{\gamma^P}{\gamma_f^P}), & \text{For } 0 \le \gamma^P < \gamma_f^P \\ 0, & \text{For } \gamma^P \ge \gamma_f^P \end{cases} \quad (3)$$

In these equations, $\emptyset_{peak}$ and $\emptyset_{res}$ are the peak and critical friction angle, respectively. As well, Ψ_{peak} is the peak dilation angle of the soil. The dilation angle (Ψ) was assumed to be equal to $\Psi = \emptyset - 30°$. As seen, the peak friction angle and peak dilation angle of soil were assumed to decrease linearly with the increase of shear plastic. Once the value of the plastic shear strain reached to the value of plastic shear strain at failure point γ_f^P (assumed to be equal to 0.1), the values of these friction and dilation angles were kept constant (Atkinson 2007).

• For the loose soil, an elastic-perfectly plastic constitutive model was considered without allowing properties of soil to change.

The above 18 cases for each fault type with three different segments thicknesses (0.35 m, 0.40 m, and 0.45 m) become together 54 cases. These 54 cases were combined

Table 3 Soil properties in the reference case

Parameter	Symbol	Unit	Dense soil	Loose soil
Elastic modulus	E_s	MPa	40	15
Peak friction angle	$\emptyset_{peak}$	°	35	30
Peak dilation angle	Ψ_{Peak}	°	5	0
Residual friction angle	$\emptyset_{residual}$	°	30	30
Soil density	ρ_s	kg/m^3	1800	1500
Poisson's ratio	v_s	-	0.30	0.30
Cohesion	c	kPa	0	0

Table 4 Segment properties in the reference case

Parameter	Symbol	Unit	Value
Density	ρ_l	kg/m^3	2500
Poisson's ratio	v_l	-	0.28
Thickness	t_l	m	0.35
Width	w_l	m	1.5
Elastic modulus	E_l	GPa	35*
Rotational stiffness of the joint	k_θ	MN.m/rad/m	100*
Maximum bending moment at the segment joint	M_{yield}	MN.m/m	0.15*
Axial stiffness of the joint	k_A	MN/m	500*
Radial stiffness of the joint	k_R	MN/m	1050*
Maximum shear forces at the segment joint	S_{yield}	MN/m	0.27
Maximum axial forces at the segment joint	T_c	MN/m	0.06

* Assumed by Do *et al.* (2014)

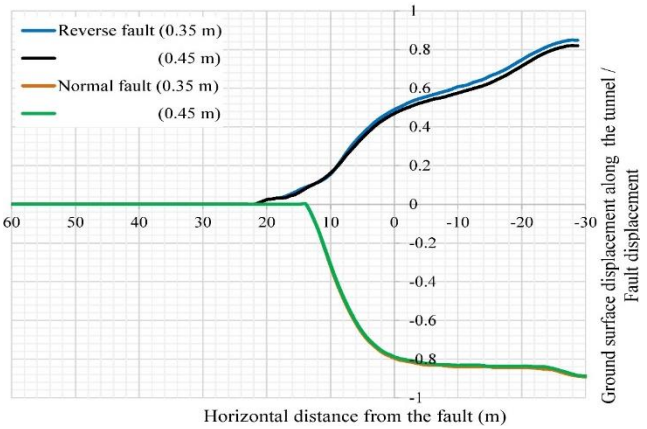

Fig. 7 Effect of the segment thickness on the ground surface displacements (the numbers in the legend of figure represent the segment thickness)

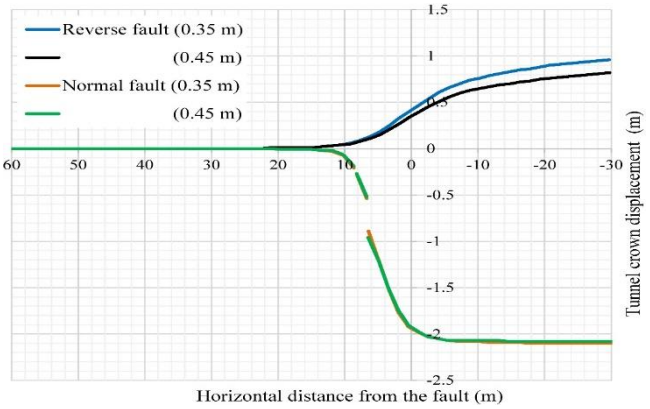

Fig. 8 Effect of the segment thickness on the tunnel crown displacements (the numbers in the legend of figure represent the segment thickness)

with different values of the faults dip angles as well as several values of the spring stiffnesses associated with the segments connections (in both directions). As the analyses were time consuming, only one case from each soil type (Table 3) with one segment type was selected (see Table 4) as the reference case. On the other hand, by combining three faults dip angles (i.e., 60°, 75°, and 90°) and six spring stiffnesses (three values for the rotational stiffness and three values for the translational stiffness between the segments), 18 cases were obtained. They were added to the obtained 54 cases to give total 72 cases.

This parametric study evaluates the effects of multiple parameters on the development of the soil plastic strains, on the deformation of the tunnel cross section, and on the displacements of the tunnel and the ground surface along the tunnel longitudinal axis, due to the fault movements.

4. Results and discussion

4.1 Effects of the segmental tunnel thickness

Comparing Fig. 6 with Fig. 7 shows how the supporting system significantly reduces the ground displacements due to having a greater stiffness than the soil. Therefore, the induced ground displacements differ from tunnel crown to ground surface in the vertical direction. That is, the maximum displacement occurs near the ground surface while the minimum is exactly above the tunnel crown. Furthermore, the ground displacements (settlement) gradually decrease from the hanging wall to the foot wall for both the normal and reverse faults. The difference between the tunnel and ground surface displacements for the reverse fault movement can be due to the fact that the tunnel structure with stiff lining significantly reduces the ground displacements. However, the ground displacements above the tunnel is a function of several factors including tunnel displacements, the displacements resulting from the fault movement acting to the soil above the tunnel, and the shear strength of the soil around the tunnel.

In the normal faulting, the induced displacement of ground surface is almost equal to the magnitude of the fault movement in the vertical direction (i.e., the fault movement is 2.5 meters, and its component in the vertical direction depends on its dip angle), which might be due to tension component of this type of faulting (soil particles cannot sustain tension forces). Hence, the maximum normalized displacement is not reached to its final limit (i.e., 1) (see e.g., Fig. 7).

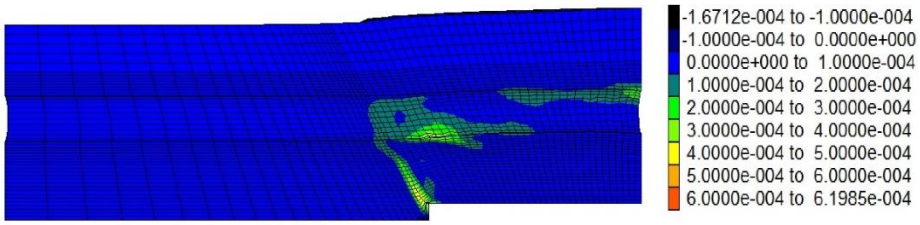

(a) Reverse fault, Segment thickness (t_l) = 0.35 m

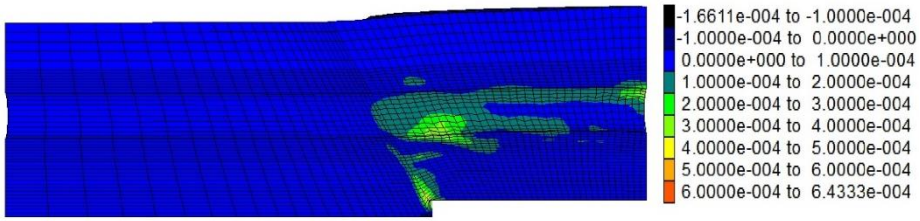

(b) Reverse fault, Segment thickness (t_l) = 0.45 m

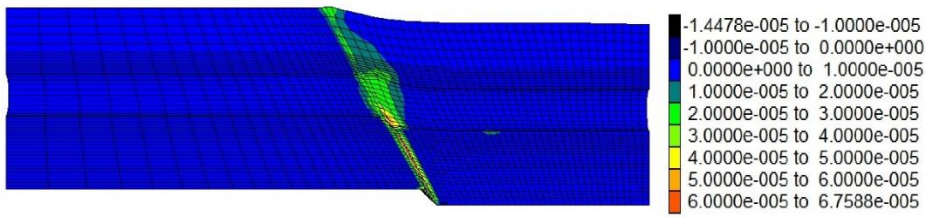

(c) Normal fault, Segment thickness (t_l) = 0.35 m

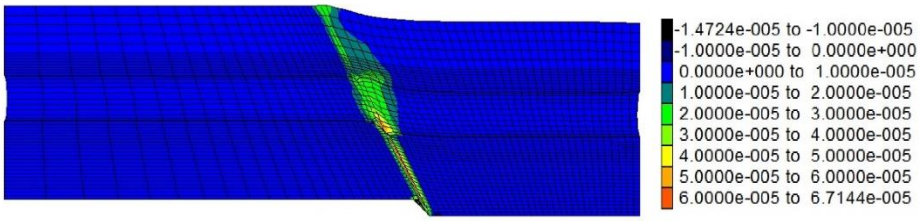

(d) Normal fault, Segment thickness (t_l) = 0.45 m

Fig. 9 Effect of the tunnel segment thickness (t_l) on the deformed mesh (the properties of the dense soil are mentioned in Table 4)

Fig. 10 Displacements of the segmental tunnel in the axial direction of the tunnel after faulting (the fault dip angle is equal to 60° and the segmental tunnel thickness is equal to 0.35 m)

Figs. 7 and 8 respectively illustrate the ground surface and the tunnel crown displacements due to the different fault movements. In the case of the reverse faulting, increasing the support system thickness (t_l) from 0.35 m to 0.45 m causes a slight decrease of the ground surface and tunnel crown displacements. In fact, a supporting system with a higher rigidity absorbs more energy, and the displacements of this system and of the ground surface above tunnel reduce. However, for the normal faulting, this is not the case. Thus, it is reasonable to enhance the tension capacity between the adjacent segments instead of increasing segments thickness (see the following sections for more details).

The other important issue is the differential settlements on the ground after faulting. When the tunnel lining thickness is equal to 0.35 m, the maximum gradient value of the ground surface displacements due to the reverse faulting offset is 0.12 (12%) which occurs at Y = 8 m (measured from the bedrock fault). For the case of the normal faulting, the gradient value is higher and is equal to 0.24 located at Y = 10 m. These values were computed for the other cases with different segment thicknesses. The results show that the location of the maximum gradient remains constant, but the value slightly decreases when a thicker segment is used

for the tunnel in the reverse faulting (e.g., for supporting system thickness equals to 0.4 m and 0.45 m, the maximum gradient values are 0.11 and 0.10, respectively) while it has no influence for the case of normal faulting offset. As a conclusion, it can be inferred that the maximum gradient of displacements in the normal faulting occurs in adjacent to the point of the intersection between the fault plane and the ground surface (before faulting).

Here, the range that the gradients of surface settlements almost equal to the maximum value is defined as the ground surface affected length which differs from the W parameter. This is the case only for normal faulting and independent of the lining thickness, e.g., 14 m (located at 0 m ≤ Y ≤ 14 m). Also, in the case of the reverse offset, the ground surface displacements occur in both of the hanging wall and the foot wall while it occurs in the hanging wall in the normal faulting (the W values, independent of the segments thickness, are respectively equal to 22 m and 14 m for the reverse and normal faulting).

In the case of the reverse fault offset, increasing tunnel lining thickness causes the plastic strains to spread out in a wider zone on the hanging wall while they are reduced on the foot wall (see Fig. 9). In fact, the more rigidity of the segment layer further prevents the tunnel from moving, and therefore, the relative displacements between the soil and the tunnel increase. For the normal faulting, it seems that increasing of the rigidity has a negligible effect on the plastic strains contour.

Fig. 10 shows how the displacements occur between the segments in the tunnel longitudinal axis (fault dip angle of 60° and segmental tunnel thickness of 0.35 m). The distance between the first and the last separated segments in the axial direction is defined as the affected length of tunnel (L_e). This parameter, independent of the segments thickness, is equal to 2.42D which is equal to nine segment rings along the tunnel axis. The maximum separation of the adjacent rings along the tunnel axis due to the normal faulting is about 0.42 m. This separation between segments can cause serious problems e.g., collapsing of soil into the tunnel, flowing of water into tunnel (if any), and finally blocking of the road. In the other type of fault, no separation occurs between segments.

4.2 Effects of the mechanical properties of soil

Several loose and dense soils with different values of density (ρ_s), the friction angle ($\emptyset$), and Elasticity Modulus (E_s) were considered in the study. As a unique value was assumed for Elasticity Modulus of the segments lining (E_l), it can be considered the output results reflect the relative elasticity modulus of the segment to the soil.

As observed in Fig. 11, there is no significant difference in the ground displacements between the loose and the dense soils in the normal faulting while this is not true in the cases of reverse faulting. That is, the displacements in the loose soil are very small compared to those of the dense soil. On the other hand, the dense soils with greater geo-mechanical properties show the greater displacements while the loose soils show the inverse trend. In fact, for the soils with greater geo-mechanical properties, in the case of the reverse faulting, the extent of the deformed meshes around

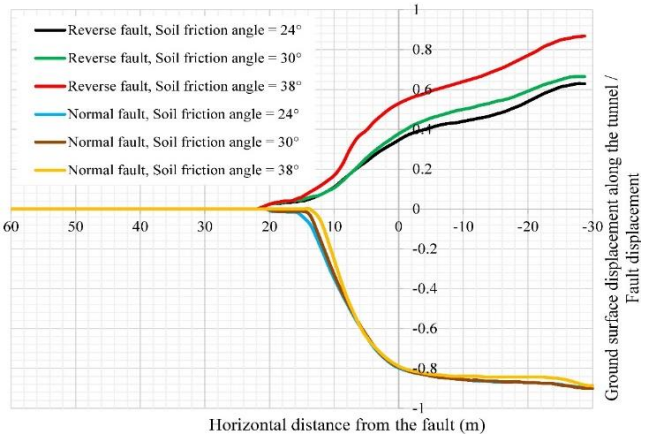

Fig. 11 Effect of the soil mechanical properties on the ground surface displacements (the soil elastic modulus for the loose and dense sand is 15 MPa and 40 MPa, respectively)

the tunnel is spread out over a wider zone but with less intensity. In the dense soils, the shear displacements tend to be localized and further limited in the zone adjacent to the fault discontinuity. But for the normal faulting, there is no significant difference between the loose and dense soils for the plastic strains considering both intensity and extent of distribution. However, unlike for the cases of the dense soil, these plastic strains spread out in both the hanging wall and the foot wall.

Analyzing this figure shows that in the loose soil with higher geo-mechanical properties, the point of maximum gradient tends to be closer to the bedrock of reverse fault. For example, in the soil with the friction angle of 24° and 30° this occurs at Y = 8 m and Y = 5 m, respectively. But ignoring this item, this location is not influenced by the value of the soil friction angle. In the normal faulting, the maximum gradient of displacements in a loose soil occurs closer to the intersection of the fault plane and the ground surface (before faulting) (Y = 12 m).

The higher geo-mechanical properties (in both of loose and dense soils as well as in two types of faulting) lead to an increase in the maximum slope of the ground surface. As a conclusion, it can be inferred that this situation can cause more damages to the buildings and structures. In fact, the highest slope of ground surface in the loose medium is much smaller than that in the dense one. For the reverse fault angle, as an example, in the soils with the friction angle of 24° and 30°, this slope is about 7% and 8% (compare it with the gradient reported in the section 4.1). The results show that the ground surface affected length is a function of soil parameters while its location depends upon the geo-mechanical parameters. That is, the higher value of soil geo-mechanical properties, the greater affected length of the ground surface. For a soil with the friction angle of 24° and the elastic modulus of 15 MPa, this value is about 17 m and occurs in 0 m ≤ Y ≤ 17 m.

It is interesting to note the W parameter is constant for all soils with different mechanical properties for the case of the reverse offset. In the loose soil case, the displacements caused by the normal fault movement spread out in the

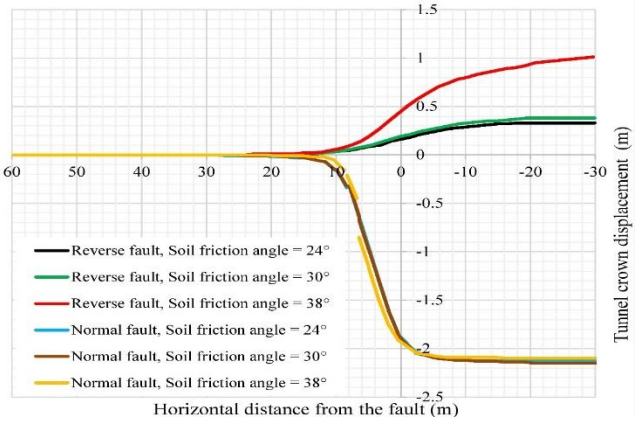

Fig. 12 Effect of the soil mechanical properties on the tunnel crown displacements (the soil elastic modulus for the loose and dense sand is 15 MPa and 40 MPa, respectively)

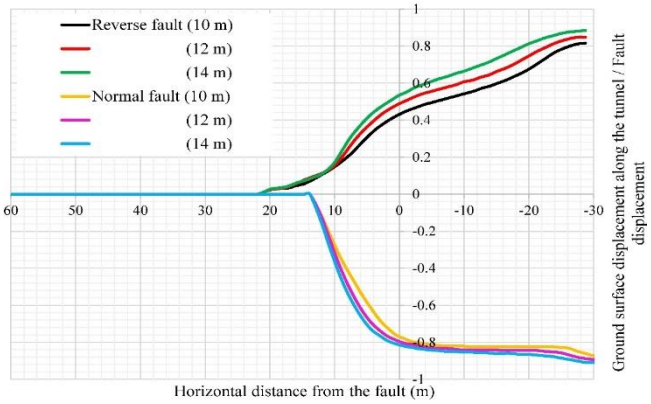

Fig. 13 Effect of the tunnel depth on the ground surface displacements (the numbers in the legend of figure represent the tunnel depth)

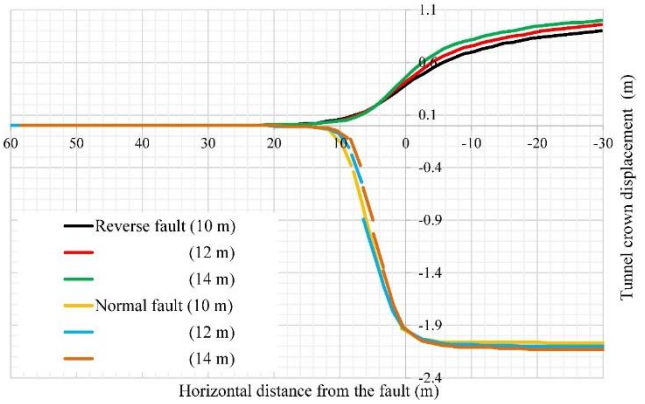

Fig. 14 Effect of the tunnel depth on the tunnel crown displacements (the numbers in the legend of figure represent the tunnel depth)

wider zone with respect to the dense soil. As well, unlike loose soil, the displacements in the dense soil occur only in the hanging wall of the normal faulting. Like the effects of the tunnel supporting system thickness (t_l), the length of tunnel affected by the normal faulting is equal to 2.42D for both the loose and the dense soils (Fig. 12). It can be seen that the maximum separation of the adjacent rings in the horizontal direction due to the normal faulting in the dense and loose soil are respectively equal to 0.42 m and 0.30 m.

4.3 Effects of the tunnel depth

Figs. 13 and 14 show, regardless of the fault type, a greater depth imposes more displacements to the ground surface while it has no influence on the W value. It implies that when the tunnel is located closer to the bedrock, its effect on controlling the ground displacements became less. In a tunnel faulted by a normal fault the location of highest surface gradient does not depend on the depth of this opening. On the other hand, both of maximum gradient value and its location have a direct relation with the tunnel burial depth. That is, increasing the burial depth from 10 m to 14 m causes the highest gradient of the ground surface to enhance about 5% for the reverse fault angle. As well, the deeper tunnels decrease the ground surface affected length. This is an important point in designing of tunnels in urban areas, and designers should take into consideration of this point on the stability of foundations, bridges, dams, and so on.

Similar to the previous results, no separation occurs between the segments of adjacent rings in the case of the reverse faulting (Fig. 14) while a remarkable impact on the profile of the tunnel crown displacements can be observed in the normal faulting i.e., the maximum horizontal separation of the adjacent rings for depths of 10 m, 12 m, and 14 m is 0.38 m, 0.42 m, and 0.44 m, respectively. It causes a discontinuous profile of the tunnel crown. In this regard, the length of tunnel affected by faulting reduces if the tunnel is located at greater depths. For tunnels at the depths of 10 m, 12 m, and 14 m, it is 2.91D, 2.42D, and 2.17D. That is, increasing the tunnel burial depth leads to increase the severity of damages due to the localization and concentration of the fault movement.

4.4 Effects of the fault dip angle

The fault dip angle (α) was increased from 60° to 90° with an increment of 15° to find out the more appreciated the tunnel angle crossing through a fault. For the reverse faulting cases, the maximum ground displacement enhances about 1.2 times when the fault dip angle is varied from 90° to 60°, meanwhile for the normal faulting, the trend is inverse i.e., increasing the fault dip angle from 60° to 90°, the maximum ground displacement intensifies about 1.1 times (Fig. 15). Similar results were obtained for the tunnel crown displacements.

For both cases of the reverse faulting and the normal faulting, the plastic strains decrease as the faults dip angle is increased. Thus, it can be inferred that the urban tunnels probably are less damaged if they pass through the dip-slip faults perpendicularly. Analyzing this figure reveals when the fault dip angle (for two types of faulting) is greater, the location of the highest surface settlement gradient tends to be closer to the intersection of the fault plane and the ground surface (before faulting). That is, the location of this gradient is located at Y = 2 m when the reverse fault dip

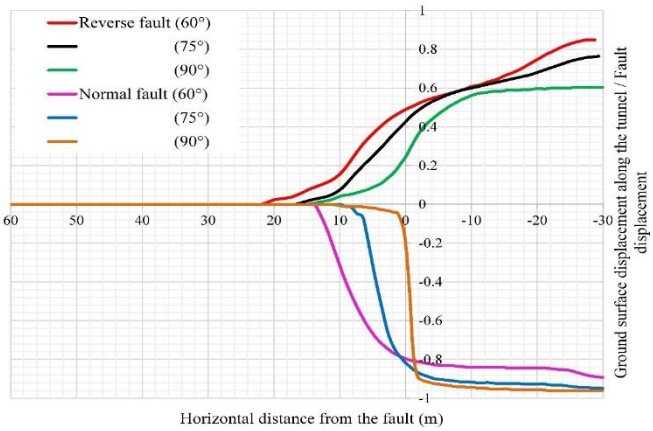

Fig. 15 Effect of the fault dip angle on the ground surface displacements (the numbers in the legend of figure represent the fault dip angle)

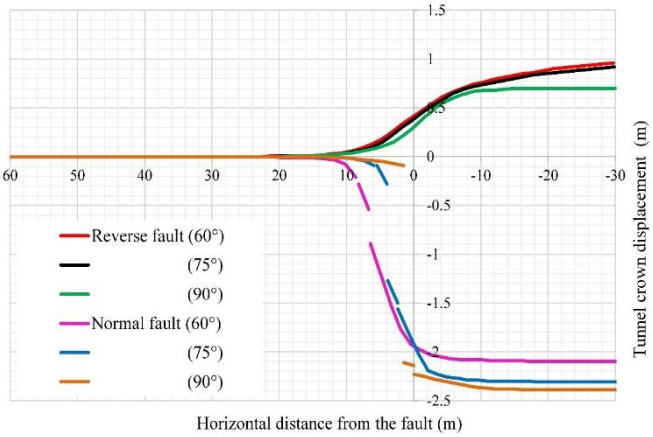

Fig. 16 Effect of the fault dip angle on the tunnel crown displacements (the numbers in the legend of figure represent the fault dip angle)

Table 5 Tunnel deformation in the horizontal and vertical directions after the dip-slip faulting

The cases	Tunnel deformation (%)			
	Reverse fault		Normal fault	
	Horizontal direction	Vertical direction	Horizontal direction	Vertical direction
The reference case of the dense soil	4.94	-5.10	4.59	-4.58
t_l = 0.40 m	3.74	-4.02	4.36	-4.42
t_l = 0.45 m	1.05	-3.21	4.07	-4.22
Dense soil, $\emptyset_{peak}$ = 36°, E_s = 40 MPa	5.03	-5.21	4.54	-4.72
Dense soil, $\emptyset_{peak}$ = 38°, E_s = 40 MPa	5.27	-5.48	4.22	-4.54
Loose soil, $\emptyset$ = 24°, E_s = 15 MPa	1.97	-2.03	0.49	-0.39
Loose soil, $\emptyset$ = 28°, E_s = 15 MPa	2.40	-2.50	0.69	-0.62
Loose soil, $\emptyset$ = 30°, E_s = 15 MPa	2.64	-2.72	0.76	-0.69
H = 10 m	5.18	-5.22	2.08	-1.54
H = 14 m	4.76	-4.89	3.28	-3.31
α = 75°	4.83	-4.95	1.69	-1.84
α = 90°	4.15	-4.32	0.03	-0.11

angle is equal to 75 degrees. This point has only about 2.7 meters difference with the point of the intersection of the fault plane and the ground surface. However, in the fault with a dip angle of 90°, the above-mentioned locations are the same (Y = 0 m).

The maximum slope of the ground surface has no direct relation with the reverse fault angle. But, the normal fault angle is a critical parameter controlling the stability of

Table 6 Rotational stiffness and rotational capacity between the segments in two directions of connection

Rotational stiffness (K_θ) (MN.m/rad/m)	Rotational capacity (MN.m/m)
100	0.15
115	0.175
132	0.20

Table 7 The effect of the rotational stiffness and the rotational capacity on the maximum tunnel deformation for the case of the normal faulting

The cases	Tunnel deformation (%)	
	Horizontal direction	Vertical direction
K_θ = 0.150 MN.m/m, H = 12 m, α = 60°	4.59	-4.58
K_θ = 0.175 MN.m/m, H = 12 m, α = 60°	2.93	-2.87
K_θ = 0.200 MN.m/m, H = 12 m, α = 60°	2.55	-2.52
K_θ = 0.150 MN.m/m, H = 12 m, α = 75°	1.69	-1.84
K_θ = 0.175 MN.m/m, H = 12 m, α = 75°	1.45	-1.64
K_θ = 0.200 MN.m/m, H = 12 m, α = 75°	1.28	-1.50
K_θ = 0.150 MN.m/m, H = 14 m, α = 60°	3.28	-3.31
K_θ = 0.175 MN.m/m, H = 14 m, α = 60°	2.91	-2.87
K_θ = 0.200 MN.m/m, H = 14 m, α = 60°	2.56	-2.49

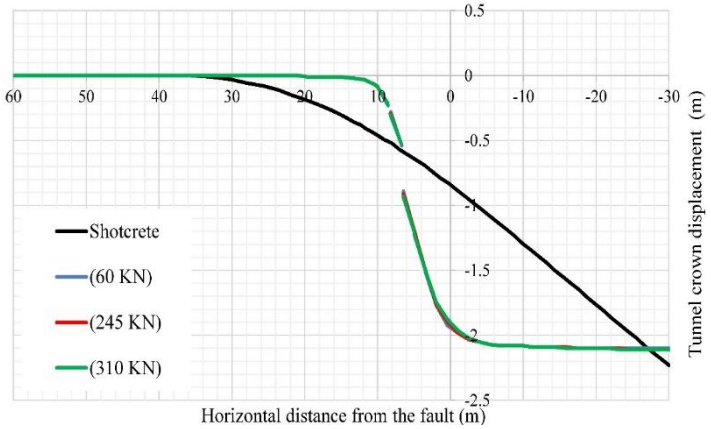

Fig. 17 Effect of the tension capacity on the displacements of the tunnel crown (the fault dip angle and the tunnel depth are 60° and 12 m, respectively)(the numbers in the legend of figure represent the tension capacity between the segments)

Table 8 The effect of tension capacity on the maximum tunnel deformation for the case of the normal faulting

The cases	Tunnel deformation (%)	
	Horizontal direction	Vertical direction
T_c = 0.060 MN, H = 12 m, α = 60°	4.59	-4.58
T_c = 0.245 MN, H = 12 m, α = 60°	4.64	-4.63
T_c = 0.310 MN, H = 12 m, α = 60°	4.66	-4.62
T_c = 0.060 MN, H = 12 m, α = 75°	1.69	-1.84
T_c = 0.245 MN, H = 12 m, α = 75°	1.78	-1.84
T_c = 0.310 MN, H = 12 m, α = 75°	1.78	-1.84
T_c = 0.060 MN, H = 14 m, α = 60°	3.28	-3.31
T_c = 0.245 MN, H = 14 m, α = 60°	3.16	-3.17
T_c = 0.310 MN, H = 14 m, α = 60°	3.20	-3.16

above-ground structures. That is, for the vertical normal fault, this slope is about 90%, but for this fault with the dip angle of 75° this value is almost 45% (Y = 5 m). In these two faults, the ground surface affected length occurs in both

of the hanging wall and foot wall. As well, the gradients of surface settlements that have values close to the maximum of this parameter occur in a smaller range. In the normal fault with the dip angle of 75° and 90°, the ground surface affected range is respectively equal to -4 m ≤ Y ≤ 6.5 m and -2 m ≤ Y ≤ 1 m.

For the normal fault offset when the dip angle is equal to 60°, 75°, and 90°, the corresponding affected length of tunnel by faulting is 2.42D, 2.10D, and 0.25D, respectively (Fig. 16).

4.5 Deformation of the tunnel cross section

In addition to consider the developed displacements, the deformation of the tunnel cross section might be a critical factor. Table 5 gives the tunnel structure deformation in the critical ring. It can be observed that

• The segments thickness is obviously the most effective parameter in controlling deformation when crossing the reverse fault;

• Construction of a tunnel in loose soils leads its deformation to decrease in both the normal and reverse faulting;

• The tunnel depth plays two different roles for the faults movements. The greater tunnel depth imposes less damage for the reverse faulting, but the results are inverse for the normal faulting;

• For both the normal and reverse faulting, increasing the fault dip angle causes the deformation of the tunnel to decrease.

4.6 Effects of the connection stiffness between the segments lining

As in the reverse fault movement, no separation occurs between the segments, the effects of the stiffness between the segments are presented for the normal faulting. The results will only be given for the depths of 12 m and 14 m and for the fault angles of 60° and 75°.

4.6.1 The rotational stiffness and the rotational capacity between the segments

For the tunnel located at depth of 12 m crossing a fault by angle of 60°, the analyses show the rotational stiffnesses (K_θ) and the rotational capacities (See table 6 for different assumed values) of segments have no effect on the ground surface and the tunnel crown displacements nor on the maximum separation between the segments. Further investigation of changing other parameters (such as the other tunnel depth and the other fault dip angle) reveals the same results. However, increasing these parameters between segments of adjacent rings results in the reduction of the tunnel deformation (Table 7). As well, the deeper tunnel with a greater fault dip angle gives the least deformation.

4.6.2 The axial stiffness and the tension capacity between the segments

The value of axial stiffness (K_a) is set to a constant value equaled to 500 MN/m, and three values for the tension capacity between the segments are selected (0.15 MN.m/m, 0.175 MN.m/m, and 0.2 MN.m/m).

The results show that this parameter does not have a significant effect on the ground surface displacements i.e., the results are similar to Fig. 7. However, increasing the tension capacity between adjacent rings leads the maximum separation between them to obviously reduce (it further resists against the fault offset) (Fig. 17). When the tension capacity between the segments in adjacent rings is increased from 0.06 MN to 0.31 MN, the maximum separation decreases from 0.43 m to 0.35 m. At the same time, the corresponding affected length of tunnel is respectively equal to 2.42D and 2.17D. Considering the infinite values for these stiffnesses will change segmental lining to the shotcrete layer, which influences the tunnel displacement as well as the tunnel profile.

For the fault dip angle equal to 75°, if the tension capacities are 0.06 MN and 0.31 MN, the maximum separation and the affected length of tunnel are 0.42 m and 0.25 m, and 2.10D and 1.89D, respectively. For deeper tunnels (14 m) which crosses the fault with an angle of 60°, an increase of the tension capacity leads to a decrease of the separation. However, the affected length of tunnel by faulting is not influenced i.e., no reduction can be seen. The details of other output results are available in Table 8.

5. Conclusions

The interaction between segmental shallow tunnels and transversely crossed dip-slip faults was investigated using 3D numerical simulations. After validation of the numerical model with the reported results of centrifuge physical tests, a parametric study was conducted to find the effects of the soil properties, the segments properties (thickness and connections stiffness), and fault dip angles on factors which influence tunnel stability and surface structures. The following conclusions can be drawn:

- Increasing the tunnel layer thickness enhances the performance of the tunnel crossing the reverse fault. This parameter leads the displacements and the deformations of both the tunnel and the ground surface to be reduced. On the other hand, changing segmental tunnel thickness has no significant effect on the tunnel displacements in the case of the normal faulting;
- For the dip-slip faulting, while the friction angle has a negligible effect, the soil stiffness has a remarkable influence on the ground surface displacements (and its gradient) and the tunnel crown displacements as well as on the deformation of tunnel cross section;
- Meanwhile increasing the tunnel burial depth crossing the reverse fault causes the displacements of the tunnel as well as the ground surface displacements to enhance and the deformation of the tunnel becomes smaller. Moreover, for the normal fault offset, increasing of this factor leads the affected length of tunnel by faulting to be reduced;
- The reverse fault dip angle is the other parameter that seems to be important in the design. When the angle between the reverse fault and the tunnel axis is high e.g., 90°, smaller displacements are imposed to the ground surface as well as the tunnel crown. But for the normal

faulting, the results are inverse. However, increasing fault dip angle leads the deformation of the tunnel to reduce;

• Except the loose soil and the fault dip angle, the other parameters have almost no effect on the position of the maximum gradient of ground surface displacements. Generally, a normal fault imposes more values in comparison to a reverse fault;

• Increasing the tension capacity between segments imposes less separation between them after the normal faulting. On the other hand, the rotational stiffness and the rotational capacity between adjacent rings have an insignificant influence on the tunnel performance.

As stated, this paper focused on the behavior of segmental tunnels crossing a dip-slip fault. Although this numerical method was conducted to fill the gaps of previous studies, some assumptions were made in this paper e.g., the surrounding soil of tunnels was considered as a dry layer with constant properties. Thus, the groundwater effects on the tunnel after faulting can be conducted in further studies. Furthermore, in reality, tunnels can cross two or more layers of soil with different properties. This condition can be investigated by using centrifuge physical tests.

Acknowledgments

The authors gratefully acknowledge the financial support by the University of Tabriz.

References

Anastasopoulos, I. and Gazetas, G. (2007), "Foundation-structure systems over a rupturing normal fault: Part II. Analysis of the Kocaeli case histories", *B. Earthq. Eng.*, **5**(3), 277-301. https://doi.org/10.1007/s10518-007-9030-9.

Anastasopoulos, I., Callerio, A., Bransby, M., Davies, M., El Nahas, A., Faccioli, E., Gazetas, G., Masella, A., Paolucci, R. and Pecker, A. (2008), "Numerical analyses of fault-foundation interaction", *B. Earthq. Eng.*, **6**(4), 645-675. https://doi.org/10.1007/s10518-008-9078-1.

Atkinson, J. (2007), *The Mechanics of Soils and Foundations*, CRC Press

Baziar, M.H., Nabizadeh, A., Lee, C.J. and Hung, W.Y. (2014), "Centrifuge modeling of interaction between reverse faulting and tunnel", *Soil Dyn. Earthq. Eng.*, **65**, 151-164. https://doi.org/10.1016/j.soildyn.2014.04.008.

Baziar, M.H., Nabizadeh, A., Mehrabi, R., Lee, C.J. and Hung, W.Y. (2016), "Evaluation of underground tunnel response to reverse fault rupture using numerical approach", *Soil Dyn. Earthq. Eng.*, **83**, 1-17. https://doi.org/10.1016/j.soildyn.2015.11.005.

Bransby, M., Davies, M. and Nahas, A.E. (2008), "Centrifuge modelling of normal fault-foundation interaction", *B. Earthq. Eng.*, **6**(4), 585-605. https://doi.org/10.1007/s10518-008-9079-0.

Bransby, M., Davies, M., El Nahas, A. and Nagaoka, S. (2008), "Centrifuge modelling of reverse fault-foundation interaction", *B. Earthq. Eng.*, **6**(4), 607-628. https://doi.org/10.1007/s10518-008-9080-7.

Cai, Q.P., Peng, J.M., Ng, C.W.W., Shi, J.W. and Chen, X.X. (2019), "Centrifuge and numerical modelling of tunnel intersected by normal fault rupture in sand", *Comput. Geotech.*, **111**, 137-146. https://doi.org/10.1016/j.compgeo.2019.03.010.

Do, N.A., Dias, D., Oreste, P. and Djeran-Maigre, I. (2014), "2D tunnel numerical investigation: the influence of the simplified excavation method on tunnel behaviour", *Geotech. Geol. Eng.*, **32**(1), 43-58. https://doi.org/10.1007/s10706-013-9690-y.

Do, N.A., Dias, D., Oreste, P. and Djeran-Maigre, I. (2014), "Three-dimensional numerical simulation for mechanized tunnelling in soft ground: The influence of the joint pattern", *Acta Geotechnica*, **9**(4), 673-694. https://doi.org/10.1007/s11440-013-0279-7.

Do, N.A., Dias, D., Oreste, P. and Djeran-Maigre, I. (2014), "Three-dimensional numerical simulation of a mechanized twin tunnels in soft ground", *Tunn. Undergr. Sp. Tech.*, **42**, 40-51. https://doi.org/10.1016/j.tust.2014.02.001.

Do, N.A., Dias, D. and Oreste, P. (2014), "2D seismic numerical analysis of segmental tunnel lining behaviour", *B. New Zealand Soc. Earthq. Eng.*, **47**(3), 206-216. https://doi.org/10.5459/bnzsee.47.3.206-216.

Do, N.A., Dias, D. and Oreste, P. (2015), "3D numerical investigation on the interaction between mechanized twin tunnels in soft ground", *Environ. Earth Sci.*, **73**(5), 2101-2113. https://doi.org/10.1007/s12665-014-3561-6.

Do, N.A., Dias, D. and Oreste, P. (2018), "Numerical investigation of segmental tunnel linings-comparison between the hyperstatic reaction method and a 3D numerical model", *Geomech. Eng.*, **14**(3), 293-299. https://doi.org/10.12989/gae.2018.14.3.293.

Do, N.A., Dias, D., Oreste, P. and Djeran-Maigre, I. (2013), "2D numerical investigation of segmental tunnel lining behavior", *Tunn. Undergr. Sp. Tech.*, **37**, 115-127. https://doi.org/10.1016/j.tust.2013.03.008.

Do, N.A., Dias, D., Oreste, P. and Djeran-Maigre, I. (2014), "2D numerical investigations of twin tunnel interaction", *Geomech. Eng.*, **6**(3), 263-275. http://doi.org/10.12989/gae.2014.6.3.263.

Do, N.A., Dias, D., Oreste, P. and Djeran-Maigre, I. (2014), "The behaviour of the segmental tunnel lining studied by the hyperstatic reaction method", *Eur. J. Environ. Civ. Eng.*, **18**(4), 489-510. https://doi.org/10.1080/19648189.2013.872583.

Gregor, T., Garrod, B. and Young, D. (2007), "Analyses of underground structures crossing an active fault in Coronado, California", *Proceedings of the World Tunnel Congress 2007 and the 33rd ITA/AITES Annual General Assembly*, Prague, Czech Republic, May.

Itasca (2005), *Fast Lagrangian Analysis of Continua in 3-Dimension (flac3d v3.1)*, Itasca Consulting Group.

Kiani, M. (2016), "Effects of surface fault rupture on shallow segmental soil tunnels-centrifuge modeling", University of Tabriz, Tabriz, Iran (in Persian).

Kiani, M., Akhlaghi, T. and Ghalandarzadeh, A. (2016), "Experimental modeling of segmental shallow tunnels in alluvial affected by normal faults", *Tunn. Undergr. Sp. Tech.*, **51**, 108-119. https://doi.org/10.1016/j.tust.2015.10.005.

Lin, M.L., Chung, C.F. and Jeng, F.S. (2006), "Deformation of overburden soil induced by thrust fault slip", *Eng. Geol.*, **88**(1-2), 70-89. https://doi.org/10.1016/j.enggeo.2006.08.004.

Lin, M.L., Chung, C.F., Jeng, F.S. and Yao, T.C. (2007), "The deformation of overburden soil induced by thrust faulting and its impact on underground tunnels", *Eng. Geol.*, **92**(3-4), 110-132. https://doi.org/10.1016/j.enggeo.2007.03.008.

Loukidis, D., Bouckovalas, G.D. and Papadimitriou, A.G. (2009), "Analysis of fault rupture propagation through uniform soil cover", *Soil Dyn. Earthq. Eng.*, **29**(11-12), 1389-1404. https://doi.org/10.1016/j.soildyn.2009.04.003.

Ng, C.W.W., Soomro, M.A. and Hong, Y. (2014), "Three-dimensional centrifuge modelling of pile group responses to side-by-side twin tunnelling", *Tunn. Undergr. Sp. Tech.*, **43**, 350-361. https://doi.org/10.1016/j.tust.2014.05.002.

Ranjbarnia, M., Zaheri, M. and Dias, D. (2020), "Three-dimensional finite difference analysis of shallow sprayed concrete tunnels crossing a reverse fault or a normal fault: A parametric study", *Front. Struct. Civ. Eng.*, **14**, 998-1011. https://doi.org/10.1007/s11709-020-0621-8.

Soomro, M.A., Ng, C.W.W., Liu, K. and Memon, N.A. (2017), "Pile responses to side-by-side twin tunnelling in stiff clay: Effects of different tunnel depths relative to pile", *Comput. Geotech.*, **84**, 101-116. https://doi.org/10.1016/j.compgeo.2016.11.011.

Wang, Z., Zhang, Z. and Gao, B. (2012), "Seismic behavior of the tunnel across active fault", *Proceedings of the 15th World Conference on Earthquake Engineering*, Lisbon, Portugal, September.

Zaheri, M., Ranjbarnia, M. and Oreste, P. (2019), "Performance of systematic fully grouted rockbolts and shotcreted layer in circular tunnel under the hydrostatic conditions using 3D finite difference approach", *Geomech. Geoeng.*, 1-14. https://doi.org/10.1080/17486025.2019.1648885.

Zaheri, M., Ranjbarnia, M., Dias, D. and Oreste, P. (2020), "Performance of segmental and shotcrete linings in shallow tunnels crossing a transverse strike-slip faulting", *Transport. Geotech.*, **23**, 100333. https://doi.org/10.1016/j.trgeo.2020.100333.

GC